



UvA-DARE (Digital Academic Repository)

Building tools for image-guided adaptive radiotherapy of bladder cancer

Chai, X.

Publication date
2012

[Link to publication](#)

Citation for published version (APA):

Chai, X. (2012). *Building tools for image-guided adaptive radiotherapy of bladder cancer*. [Thesis, fully internal, Universiteit van Amsterdam]. Boxpress.

General rights

It is not permitted to download or to forward/distribute the text or part of it without the consent of the author(s) and/or copyright holder(s), other than for strictly personal, individual use, unless the work is under an open content license (like Creative Commons).

Disclaimer/Complaints regulations

If you believe that digital publication of certain material infringes any of your rights or (privacy) interests, please let the Library know, stating your reasons. In case of a legitimate complaint, the Library will make the material inaccessible and/or remove it from the website. Please Ask the Library: <https://uba.uva.nl/en/contact>, or a letter to: Library of the University of Amsterdam, Secretariat, P.O. Box 19185, 1000 GD Amsterdam, The Netherlands. You will be contacted as soon as possible.

Chapter 6

Semiautomatic bladder segmentation on CBCT using a population based model for multiple plan ART of bladder cancer

Xiangfei Chai, Marcel van Herk, Anja Betgen, Maarten Hulshof and Arjan Bel

Physics in Medicine and Biology (to be re-submitted with revision)

Abstract:

Purpose: The aim of this study is to develop a novel semiautomatic bladder segmentation approach for selecting the appropriate plan from the library of plans for a multiple plan adaptive radiotherapy (ART) procedure.

Materials and Methods: A population based statistical bladder model was first built from the training data set (95 bladder contours from 8 patients). This model was then used as constraint to segment bladder in an independent validation data set (233 CBCT scans from the remaining 22 patients). All 3D bladder contours were converted into parametric surface representations using spherical harmonic expansion. Principal component analysis (PCA) was applied in the spherical harmonic based shape parameter space to calculate the major variation of bladder shapes. The number of dominating PCA modes was chosen such that 95% of the total shape variation of the training data set was described. The automatic segmentation started from bladder contour of the planning CT of each patient, which was modified by changing the weight of each PCA mode. As a result, the segmentation contour was deformed consistently with the training set to best fit the bladder boundary in the localization CBCT image. A cost function was defined to measure the goodness of fit of the segmentation on the localization CBCT image. The segmentation was obtained by minimizing this cost function using a simplex optimizer. After automatic segmentation, a fast manual correction method was provided to correct those bladders (parts) that were poorly segmented. Volume and distance based metric and the accuracy of plan selection from multiple plans were evaluated to quantify the performance of the automatic and semiautomatic segmentation methods.

Results: For the training data set, only 7 PCA modes were needed to represent 95% of the bladder shape variation. The mean CI overlap and residual error (SD) of automatic bladder segmentation over all of the validation data is 70.5% and 0.39 cm, respectively. The agreement of plan selection between automatic bladder segmentation and manually delineation was 56.7%. The automatic segmentation and visual assessment took on average 7.8 seconds(s) and 9.7 s, respectively. In 53.4% of the cases, manual correction was performed after automatic segmentation. The manual correction improved the mean CI overlap, mean residual error, and plan selection agreement to 77.7%, 0.30 cm and 80.7%, respectively. Manual correction required on average 8.4 markers and took on average 35.5 seconds.

Conclusion: The statistical shape based segmentation approach allows automatic segmentation of bladder on CBCT with moderate accuracy. Limited user intervention can quickly and reliably improve the bladder contours. This segmentation method is suitable to select the appropriate plan for a multiple plan ART of bladder cancer.

6.1 Introduction

One of the major factors limiting the precision of the radiotherapy for bladder cancer is organ motion. The inter- and intra- fractional movement of the bladder wall can be as much as 3 cm due to changes in volume of bladder and adjacent organs [15;18]. Various groups have developed multiple plan adaptive radiotherapy (ART) strategies for bladder cancer, which enable to correct the position and deformation of the target [22;23;29;55;56;130]. In these treatment strategies, multiple plans with different bladder volumes are created offline based on multiple planning CT or CBCT images acquired early on during or before treatment. Subsequently, the smallest plan safely covering the bladder on CBCT is then selected online as the plan of the day. All of these groups have reported that compared to the offline adaptive plan or traditional planning, the multiple plan ART improves coverage of the bladder CTV and reduces the amount of small bowel irradiated, potentially reducing side effects [22;23;29;54-56].

However, two key hurdles prevent the widespread implementation of the multiple plan ART strategy. First, extra bladder delineation on CT or CBCT images for multiple plans generation is quite labor intensive. The published multiple plan ART strategies require two to five extra bladder contours to generate the library of plans, which significantly increases technician's workload. The second hurdle is that online manual plan selection at the treatment console immediately before treatment is not an easy judgment in practice due to the complexity of patient anatomy and the low soft tissue contrast of CBCT.

To facilitate the more widespread clinical implementation of multiple plan ART of bladder cancer, an automatic bladder segmentation approach for robust plan selection was previously developed in our group [131]. In that method, a statistical bladder model was built for each patient to describe the patient-specific bladder shape variation and this patient-specific model was then used to segment the bladder on localization CBCT images. That statistical shape based segmentation approach was robust enough to handle the relatively poor CBCT image quality and allowed for fast and reliable automatic segmentation of bladder on CBCT.

A drawback of our previous segmentation method is that it can only work after collecting the first five CBCT images for each patient. It requires manual delineation of five bladder contours and hence is not applicable for multiple plan ART strategies that start from the first treatment day [23;29;55;56]. Moreover, the patient-specific model based on the first six images cannot guarantee a good representation of all other treatment days. Our previously developed segmentation approach fails in 8% of the cases. Hence, after automatic segmentation, a visual assessment of the segmentation result is necessary and a quick manual correction may be needed to edit the segmented bladder.

In the present study, we have developed a novel bladder segmentation method using a population based bladder shape model, combined with quick manual correction. Contrary to the previous method [131], the new method in this paper use single generic model for all segmentation instead of having to build patient-specific model for each patient. This method consisted of offline model-building and online

segmentation steps. After the automatic segmentation, a limited user intervention was added in the new method to correct the poorly segmented bladder.

The aim of this study is to present a more viable semiautomatic segmentation method and study its ability for selecting the appropriate plan from the library of plans for a multiple plan ART procedure.

6.2 Materials

6.2.1 Patient and image data

From July 2007 to March 2008, 8 male bladder cancer patients with lipiodol markers were treated at the Department of Radiation Oncology of Academic Medical Center, University of Amsterdam. All 8 patients received partial bladder treatment with full bladder drinking protocol. Each patient received one planning CT scan and 8-13 (average 10.9) follow up CT and CBCT scans. The bladder contours of all the 95 CT and CBCT scans from these 8 male patients were manually delineated by one observer. These 95 bladder contours were included in the training data set to build a population based statistical bladder model.

The data used for bladder segmentation is same as the data in previous study [131]. The data is also acquired at the Department of Radiation Oncology of the Netherlands Cancer Institute-Antoni van Leeuwenhoek Hospital from October 2003 to July 2006, but only the data of male patients was selected. Twenty-two male patients with one planning CT and 5-19 (average 10.6) CBCT scans were included into the validation data set of this study. Fourteen out of the 22 included patients received partial bladder treatment with full bladder drinking protocol and the remaining 8 patients received whole bladder treatment with empty bladder drinking protocol. The bladder contours of planning CT were used as the input for the segmentation method. The bladder contours of all 233 CBCT scans were used to validate the bladder segmentation algorithm.

All slice-by-slice delineated bladder contours from both training and validation data sets were converted to 3D surface meshes consisting of vertices and triangular connections. The 3D surface mesh was smoothed with three iterations using a simple umbrella operator [122] to eliminate unnatural shape differences between different slices.

6.3 Methods

The proposed segmentation method consists of major components, i.e., offline statistical shape model building and online bladder segmentation. A population based statistical bladder shape was calculated from a spherical harmonics description of a large set of training bladder samples from CT or CBCT images. Bladder segmentation was then performed on localization CBCT images, which were independent from the training data.

Compared with the previous segmentation method, the proposed method only required a generic bladder model that is built once instead of having to build a patient-specific bladder model for each patient. The proposed method also includes a fast manual segmentation correction, which does not exist in the previous method.

6.3.1 Generic bladder model

6.3.1.1 Principal of spherical harmonic expansion

We chose to use the coefficients from the Laplace series harmonic expansion of delineation as the shape descriptors presented by Brechhuler et al. [132]. The Laplace series is a generalized Fourier series in spherical coordinates. It expands any spherical surface function $\mathbf{v}=(x(\theta, \phi), y(\theta, \phi), z(\theta, \phi))^T$ as the sum of spherical harmonics basis functions over the unit sphere:

$$\mathbf{v} = \sum_{l=0}^{\infty} \sum_{m=-l}^l \omega_l^m Y_l^m(\theta, \phi) \quad \theta \in [0; \pi], \phi \in [0; 2\pi) \quad (6.1)$$

where the coefficients ω_l^m are three dimensional vectors due to the three coordinate functions. The spherical harmonic basis function Y_l^m is defined as:

$$Y_l^m(\theta, \phi) = \sqrt{\frac{2l+1}{4\pi} \frac{(l-m)!}{(l+m)!}} P_l^m(\cos \theta) e^{im\phi} \quad (6.2)$$

$$Y_l^{-m}(\theta, \phi) = (-1)^m Y_l^{m*}(\theta, \phi) \quad (6.3)$$

where $-l \leq m \leq l$ of degree l and order m and Y_l^{m*} denotes the complex conjugate of Y_l^m and P_l^m the associated Legendre polynomials

$$P_l^m(x) = \frac{(-1)^m}{2^l l!} (1-x^2)^{\frac{m}{2}} \frac{d^{m+l}}{dx^{m+l}} (x^2-1)^l \quad (6.4)$$

The coefficients ω_l^m are obtained by solving a least-squares problem [133].

6.3.1.2 Spherical harmonic expansion of bladder contours

We chose the planning CT of the first patient in the training data set as the reference. All other CT and CBCT scans from the training data set were first registered to the reference scan using the pelvic bone using both translations and rotations without scaling. Subsequently, the registration was done again using just pubis bone with only translation. After both registrations were complete, all of the bladder contours were aligned by pubis bone (figure 6.1). We manually found a reference point (red star in figure 6.1), which was situated inside all bladder contours and the entire surface of each bladder could be “seen” from this point. The reference point is 2.65 cm above and 2.62 cm behind the center of pubis bone (yellow star in figure 6.1). A uniform sphere contour with $L=2091$ evenly distributed vertices was created (green circle in figure 6.1) and centered on the defined reference point. The N ($N=95$) bladder contours in the training data set were then re-sampled at the intersection of radial lines passing through the reference point and bladder contours.

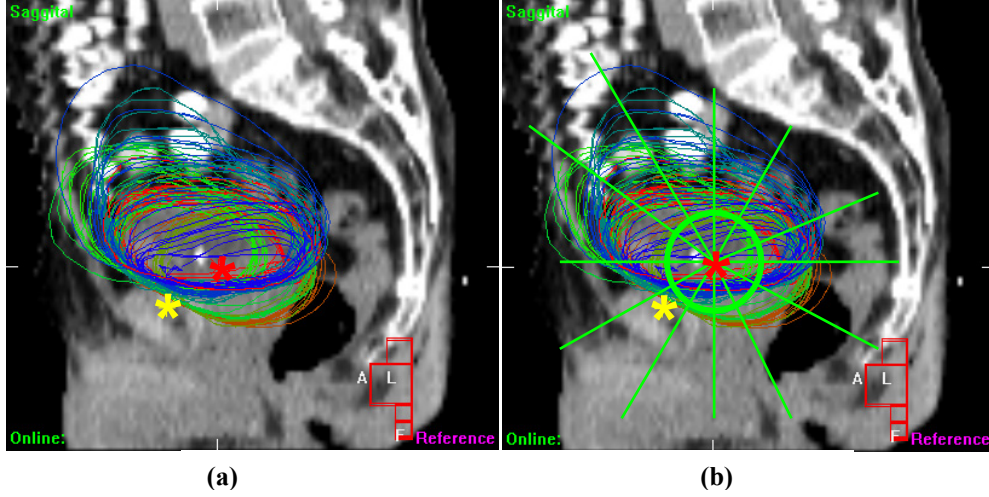


Figure 6.1: (a) 95 bladder contours from 8 patients used to construct bladder model, overlaid on the reference planning CT. Each color indicates the contours of one patient. A reference point (red star) is located inside all of the contours and a yellow star is in the center of pubis bone. (b) The 95 bladder contours are re-sampled in radial direction from the reference point.

After the re-sampling over a unit sphere, the original surface shape vector was represented by a sphere surface function $\mathbf{v} = (x(\theta, \phi), y(\theta, \phi), z(\theta, \phi))^T$. We applied the spherical harmonic expansion to all bladder sphere surfaces $\mathbf{v}(1), \mathbf{v}(2), \dots, \mathbf{v}(N)$ ($N=95$). The shape description coefficients vector $\omega = \{\omega(i)\}_{i=1,2,\dots,N}$ consists of all spherical harmonic coefficient $\omega(i)$ up to degree K $\omega(i) = (\omega(i)_{x0}^0, \omega(i)_{y0}^0, \omega(i)_{z0}^0, \omega(i)_{x1}^{-1}, \omega(i)_{y1}^{-1}, \omega(i)_{z1}^{-1}, \dots, \omega(i)_{xK}^K, \omega(i)_{yK}^K, \omega(i)_{zK}^K)^T$. The degree of harmonics determines the upper limit of spatial variation that can be modeled, i.e., the higher degree used, the higher level of detail of bladder surface can be represented. We computed the spherical harmonic expansion for all bladder sphere surfaces using degree K from 1 up to 17.

Using K degree harmonics, a new bladder surface $\mathbf{v}^{[K]}$ was reconstructed by computing the inversed spherical harmonic transformation (ISHT) using coefficients ω as input:

$$\mathbf{v}^{[K]} = ISHT(\omega) = \sum_{l=0}^K \sum_{m=-l}^l \omega_l^m Y_l^m(\theta, \phi) \quad (6.5)$$

The residual error of spherical harmonic expansion with degree K to represent the bladder shape was measured by calculating the difference $\mathbf{e}^{[K]}$

$$\mathbf{e}^{[K]} = \mathbf{v}^{[K]} - \mathbf{v} \quad (6.6)$$

The mean residual error overall L vertex of N contours is

$$\mathbf{R}^{[K]} = \frac{1}{N} \sum_{i=1}^N \left(\frac{1}{L} \sum_{j=1}^L \|\mathbf{e}_{i,j}^{[K]}\| \right) \quad (6.7)$$

where $\|\mathbf{e}_{i,j}^{[K]}\|$ is the vector length of 3D vector $\mathbf{e}_{i,j}^{[K]}$.

The degree K was chosen such that the mean residual error $\mathbf{R}^{[K]}$ over all bladder surface representations was smaller than 1 mm.

6.3.1.3 PCA based statistical bladder model

Using the spherical harmonic expansion, the Cartesian coordinate information of 2091 vertices in each re-sampled bladder contour can be represented by a shape parameter vector $\omega(i)$ with $3*(K+1)^2$ coefficients. Given the N ($N=95$) aligned bladder surfaces in the training data set, the shape parameter vector $\omega = \{\omega(i)\}_{i=1,2,\dots,N}$ could be seen as samples from a random process and N shape parameter vectors $\omega(i)$ correlated to each other. Hence, the dimensionality of the shape parameter vector can be further reduced by computing the major modes of shape variation through principal component analysis (PCA) [83;134].

The shapes of the deformed organ were decomposed by a mean shape and a weighted sum of N eigenmodes:

$$\omega = \omega_0 + \sum_{n=1}^N \psi_n \mathbf{q}_n, \quad \|\mathbf{q}_n\| = 1 \quad (6.8)$$

where ω_0 was the mean shape parameter vector, and vectors \mathbf{q}_n were the eigenvectors of covariance matrix of input data ω , corresponding to the N eigenvalues λ_n . The coefficients ψ_n were normally distributed random variables with zero means and corresponding eigenvalues λ_n as variances.

The dominating eigenmodes, i.e., the eigenmodes with largest eigenvalues, represented the major bladder deformation patterns. The eigenvalues were normalized by dividing each eigenvalue by the sum of all eigenvalues:

$$\lambda'_i = \frac{\lambda_i}{\sum_{j=1}^N \lambda_j} \quad (6.9)$$

The sum of all N ($N = 95$) eigenvalues was considered as 100% of the bladder shape variation. The number of eigenmodes D was chosen such that 95% of the bladder shape variation was described. The D eigenmodes were used to guide the bladder segmentation on localization CBCT scans.

6.3.2 Bladder segmentation guided by statistical bladder model

6.3.2.1 Automatic bladder segmentation

The bladder segmentation on localization CBCT used the following two assumptions. First, that the dominating PCA modes of bladder shape variation calculated from the training data set were representative of the bladder shape variation in the validation data set. Second, that the directional gradient field of the planning CT sampled by its bladder vertices was correlated with the directional gradient field of the localization CBCT sampled by the corresponding bladder vertices.

The inputs of the segmentation method includes the reference CT from the training set, several dominating PCA modes, a localization CBCT, and the planning CT with its

bladder contour from the same patient as the localization CBCT. In order to suppress noise, a 3D recursive Gaussian smoothing filter [124] with a standard deviation 2 mm was applied to both planning CT image and localization CBCT image

The planning CT was first registered to the reference CT from training data set using the pubis bone in order to transform the reference point to the planning CT. From this reference point, the bladder contour of the planning CT was re-sampled along radial directions as \mathbf{c}_0 . The localization CBCT was then registered with the planning CT using the entire pelvic bone. After the registration, the re-sampled bladder contour \mathbf{c}_0 from planning CT was mapped to localization CBCT as the initial shape of the bladder segmentation $\mathbf{c}_0^*(\{\mathbf{P}_i = 0\}_{i=1,\dots,D})$.

For the purpose of calculating the directional gradient field, extra interior and exterior bladder contours \mathbf{c}_{int} and \mathbf{c}_{ext} were created by shrinking and expanding the vertices of the bladder contour \mathbf{c}_0 by 5 mm along a direction normal to each vertex. These 3D contours \mathbf{c}_0 , \mathbf{c}_{int} and \mathbf{c}_{ext} all had L ($L=2091$) vertices and same triangular surface connections.

The bladder segmentation contour $\mathbf{c}_0^*(\mathbf{P})$ on the localization CBCT image started from the bladder contour \mathbf{c}_0 in planning CT, where $\mathbf{c}_0^*(\{\mathbf{P}_i = 0\}_{i=1,\dots,D}) = \mathbf{c}_0$. The shape parameters vector $\mathbf{P} = \{\mathbf{P}_i\}_{i=1,\dots,D}$ contains the weights of the D dominating PCA modes $\mathbf{Q} = (q_1, q_2, \dots, q_D)^T$ in spherical harmonic space. A shape function $\mathbf{P} \cdot \mathbf{Q}$ in spherical harmonic space was converted to a shape function in Cartesian space by inversed spherical harmonic transformation as in equation (6.5). The bladder segmentation contour $\mathbf{c}_0^*(\mathbf{P})$ is the sum of initial bladder contour \mathbf{c}_0 and bladder deformation $ISHT(\mathbf{P} \cdot \mathbf{Q})$:

$$\mathbf{c}_0^*(\mathbf{P}) = \mathbf{c}_0 + ISHT(\mathbf{P} \cdot \mathbf{Q}) \quad (6.10)$$

As a result, when changing the shape parameter vector \mathbf{P} , the initial bladder contour \mathbf{c}_0 deforms according to the deformation pattern calculated from the training data set.

Similarly, for the calculation of directional gradient field, interior contour candidate $\mathbf{c}_{\text{int}}^*(\mathbf{P})$ and exterior contour candidate $\mathbf{c}_{\text{ext}}^*(\mathbf{P})$ were also created by shrinking and expanding the vertices of contour candidate $\mathbf{c}_0^*(\mathbf{P})$ by 5 mm along a direction normal to each vertex.

A cost function E was defined to measure how well the deformed bladder contour matched the underlying bladder edge on the localization CBCT image. The cost function E was the sum of the cross correlation (CC) between the directional (interior and exterior) gradient field of the planning CT sampled on its corresponding bladder contour and the directional (interior and exterior) gradient field of the localization CBCT sampled on the segmentation contour candidate.

$$E = CC(G_P^{\text{int}}, G_V^{\text{int}}) + CC(G_P^{\text{ext}}, G_V^{\text{ext}}) \quad (6.11)$$

The cross correlation between two gradient field G_P and G_V is

$$CC(G_P, G_V) = \frac{\sum_{i=1}^L (G_P(i) - \bar{G}_P)(G_V(i) - \bar{G}_V)}{\sqrt{\sum_{i=1}^L (G_P(i) - \bar{G}_P)^2} \sqrt{\sum_{i=1}^L (G_V(i) - \bar{G}_V)^2}} \quad (6.12)$$

The interior gradient field of planning CT G_P^{int} , interior gradient field of localization CBCT G_V^{int} , exterior gradient field of planning CT G_P^{ext} and exterior gradient field of localization CBCT G_V^{ext} were calculated by the difference between the images intensity sampled by the original bladder contour and the images intensity field sampled by the interior and exterior bladder contour.

In (6.11), $G_P^{\text{int}} = I_P(\mathbf{c}_0) - I_P(\mathbf{c}_{\text{int}})$, $G_P^{\text{ext}} = I_P(\mathbf{c}_0) - I_P(\mathbf{c}_{\text{ext}})$, $G_V^{\text{int}} = I_V(\mathbf{c}_0^*) - I_V(\mathbf{c}_{\text{int}}^*)$ and $G_V^{\text{ext}} = I_V(\mathbf{c}_0^*) - I_V(\mathbf{c}_{\text{ext}}^*)$, where I_P and I_V represent the intensity field of the planning CT and localization CBCT images.

The segmentation process needs to find the shape parameter vector \mathbf{P}' that best represents the bladder surface in a validation image:

$$\mathbf{P}' = \arg \min(E | \mathbf{P}) \quad \mathbf{P}'_i \in [-3\sigma_i, 3\sigma_i], \quad (6.13)$$

where σ_i is the square root of the eigen value λ_i . The search for the optimum shape parameter vector was carried out by a simplex optimizer within the interval $[-3\sigma, 3\sigma]$ to minimize the cost function of E .

6.3.2.2 Manual correction after automatic segmentation

Due to the artifacts of CBCT, inconsistent gradient values of the bladder edge between CT and CBCT, and non-global optimized cost functions, sometimes the proposed method could fail to correctly segment the bladder on CBCT. Hence, after automatic segmentation, the user was required to roam through the sagittal planes and visually assess whether the segmentation fit the bladder edge of validation CBCT image well. If the bladder was incorrectly segmented, the user could manually add several markers on the edge of the bladder where automatic segmentation mismatched. With these manually defined markers, an extra term $\alpha E_{\text{External}}$ was introduced into the cost function E :

$$E^* = E + \alpha E_{\text{External}} \quad (6.14)$$

The E_{External} is the average distance from the markers to bladder segmentation surface. Note that α is a weighting parameter. We determined the optimum value of α by conducting a parametric study using the entire validation data set. For each values of

α , we computed the segmentation error. The value that yielded minimal segmentation error was chosen as the optimum value of α . The same α value was used for all validation data.

After several markers were set on the edge of the bladder, the user could re-segment the bladder using cost function E^* that included both the edge and marker fitting. The new segmentation also used a simplex optimizer and started from the bladder contour of the planning CT. After the new segmentation, the user would re-assess and add additional markers until a satisfactory result was achieved.

The automatic segmentation time, assessment time, frequency of manual correction, number of manually defined makers, and manual correction time were recorded.

6.3.3 Validation of bladder segmentation

To evaluate the performance of the automatic and semiautomatic bladder segmentation methods, we calculated volume and distance based errors and accuracy of plan selection from library of plans using automatic bladder segmentation.

We used the conformity index (CI) to measure the volume overlap between the segmented bladder and manually delineated bladder. For two regions R_1 and R_2 , the CI was defined as the ratio of the volume of intersection to the volume of union between R_1 and R_2

The signed local residual error was defined by computing the distance of the position in manually delineated bladder surface to the triangles in segmented bladder surface. The residual error was positive when the point from the manually delineated bladder surface was located outside the segmented bladder and negative when the point from the manually delineated bladder surface was located inside the segmented bladder. Note that the manually delineated bladder after smoothing is used for volume and distance based metrics calculation.

The bladder volume and the segmentation errors of patients on different protocols (whole bladder radiation and partial bladder radiation) were recorded separately.

Besides the volume and distance based conformity test, the accuracy of plan selection using automatic segmentation was also calculated. For each patient, three plans with different PTV volume were created from the first six scans, according to the protocol proposed by Foroudi et al. [54]. The small PTV was the smallest bladder of the six bladders with additional 5 mm uniform margin. The large PTV was the Boolean addition of all the six bladders with additional 5 mm uniform margin. In literature [54], the medium PTV was visually determined for each axial slice, from the largest and smallest bladders, using a ruler tool as a guide. However, in our study, for the sake of simplicity and reproducibility, instead of the visually determined contour the medium PTV was defined by the Boolean addition of the smallest F bladders out of the six bladders with additional 5 mm uniform margin. F was chosen such that the F th smallest bladder has the closest volume to the median volume of the largest and smallest bladders.

For each validation CBCT scan, the plan for smallest PTV of the three plans which can safely cover 99% of the bladder volume was selected as the plan of the day. We separately used the manually delineated bladder and segmented bladder to select the appropriate plan. In total, there were four possible cases: either the plan for small, medium, or large PTV was selected or none of the three plans was sufficient to cover 99% of the bladder volume. We considered the optimal plan selected by the manually delineated bladder as the reference standard. The agreement between the plans selected by the automatically segmented bladders and reference standard was recorded.

6.4 Results

We computed the spherical harmonic expansion for all bladder sphere surfaces by varying the degree K from 1 up to 17. An example of the spherical harmonic expansion was illustrated in figure 6.2. We observed that when the bladder delineation was expanded to only the first degree ($K=1$) harmonics, the reconstructed shape was a simple ellipsoid which approximates the coarse shape of the bladder. At higher K , the reconstructed shape better approximated the original bladder shape. A spherical harmonic function with degree of five provides a good approximation of the original bladder shape (figure 6.3), since the mean residual error was smaller than 1 mm. Consequently, $K=5$ was chosen.

The dimension of the coefficients $\omega(i)$ in equation (6.5) is given as $3*(K+1)^2$, so for the selected degree $K=5$, 108 parameters are needed to describe the bladder shape. For the given training set of bladder contours, the dimensionality of the shape parameter space was further reduced to 7 using principal component analysis. These 7 PCA modes represent more than 95% (96.3%) of the bladder shape variation (figure 6.4). Figure 6.5 visualizes the first 7 dominating PCA modes. The first mode is associated with bladder volume change. The second and third modes mainly model translations and rotations. The fourth, fifth, sixth and seventh modes model other deformation patterns.

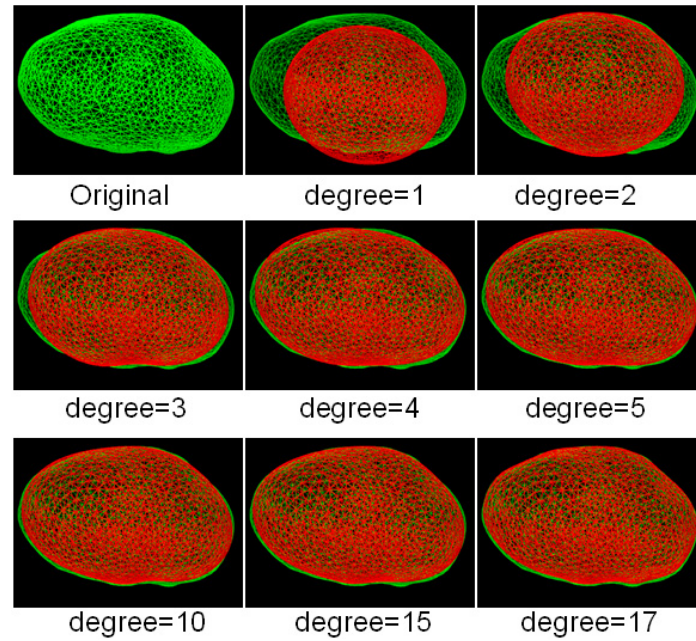


Figure 6.2: Example of spherical harmonic shape expansion of a bladder for 8 different degrees.

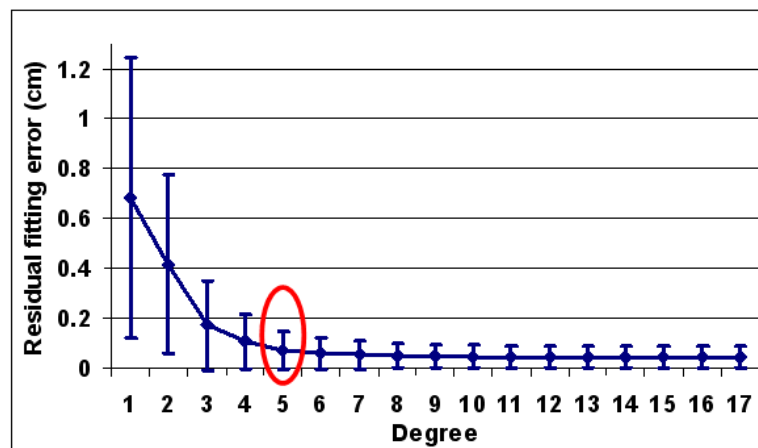


Figure 6.3: The mean and standard deviation (error bar) of spherical harmonic shape expansion of bladder as a function of degree.

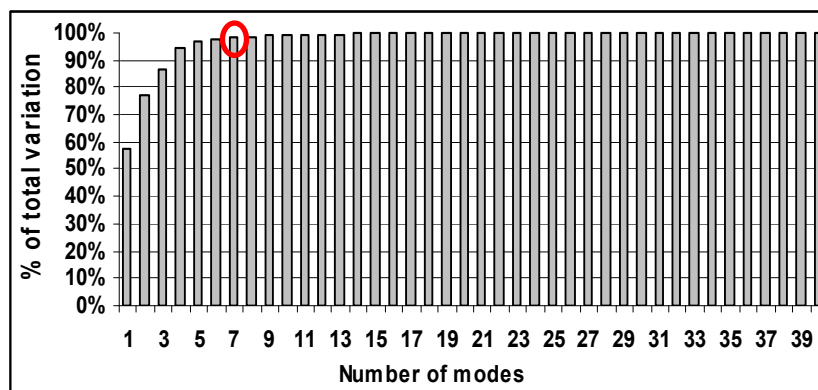


Figure 6.4: The integral of the eigenvalues for the training data set as function of the number of PCA modes. The sum of all eigenvalues was normalized to 100%.

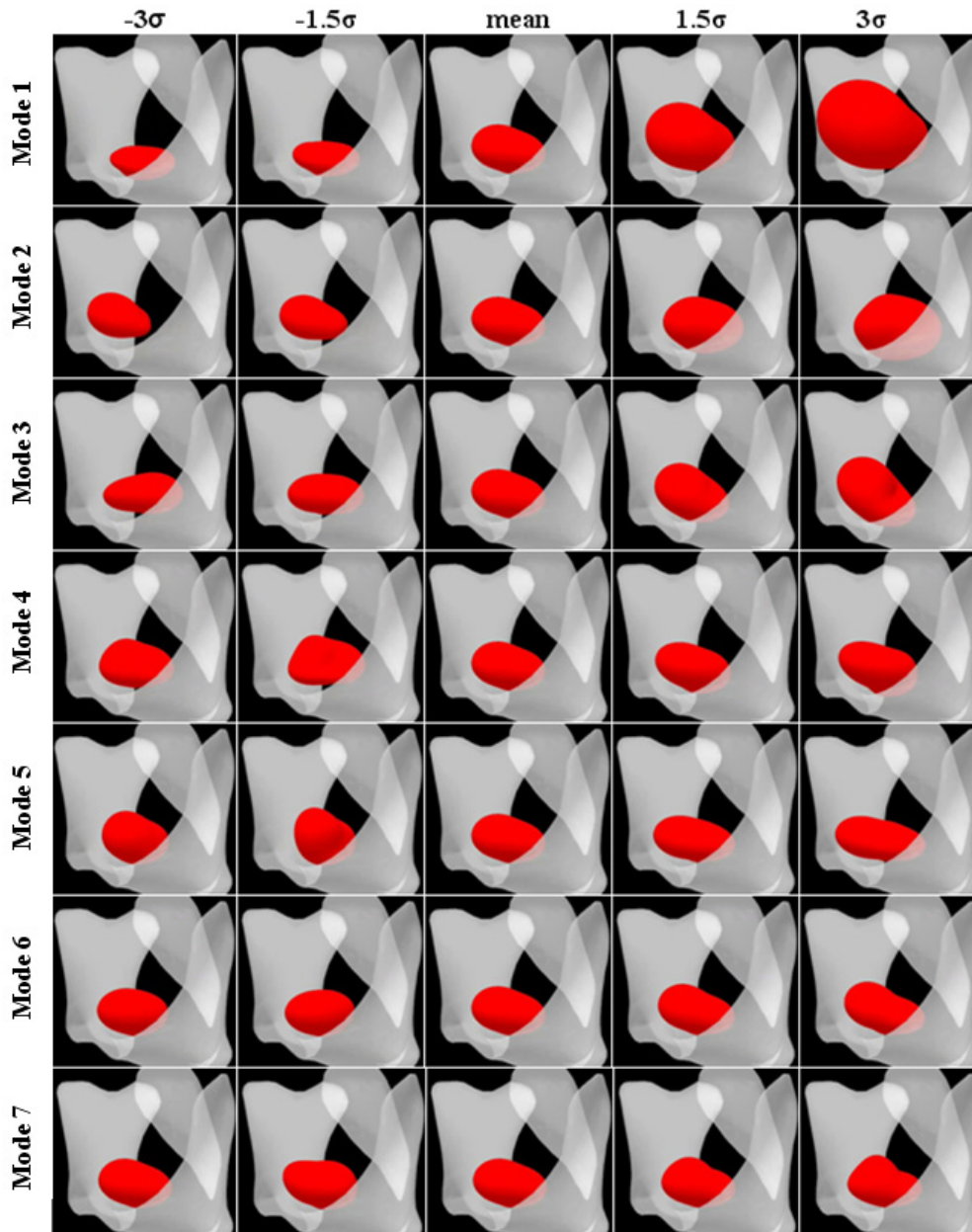


Figure 6.5: The seven dominating PCA modes of shape variation derived from 95 bladder shapes in the training data set. The red surface in the middle of each picture is the surface of bladder. The white structures are the spine and pelvic bone. The central column represents the mean bladder shape, whereas the right and left two columns are bladder shapes with plus and minus 1.5 and 3 times the standard deviation of the shape variation in each mode.

For bladder segmentation on all 233 localization CBCT images, the automatic segmentation took on average 7.8 seconds on a personal computer equipped with Core 2 Duo CPU of 3.0 GHz and 4 GB of RAM. Visual assessment of the segmentation took on average 9.7 seconds. In 53.4% of the cases, manual correction was performed after automatic segmentation. For segmentations that required manual correction, on average 8.4 markers were placed and the procedure took on average 35.5 seconds longer.

Figure 6.6 shows an example of a successful automatic bladder segmentation with manual bladder delineation and three different PTVs from the library of plans. An example of failed automatic bladder segmentation is illustrated in figure 6.7 (a). After

manually placing several markers on the visible edge of the bladder, the incorrectly segmented bladder was corrected to correspond with the actual bladder edge (figure 6.7 (b)). The average absolute residual error distribution over all 233 bladder segmentations illustrates a higher segmentation residual error in the posterior parts of the bladder (figure 6.8).

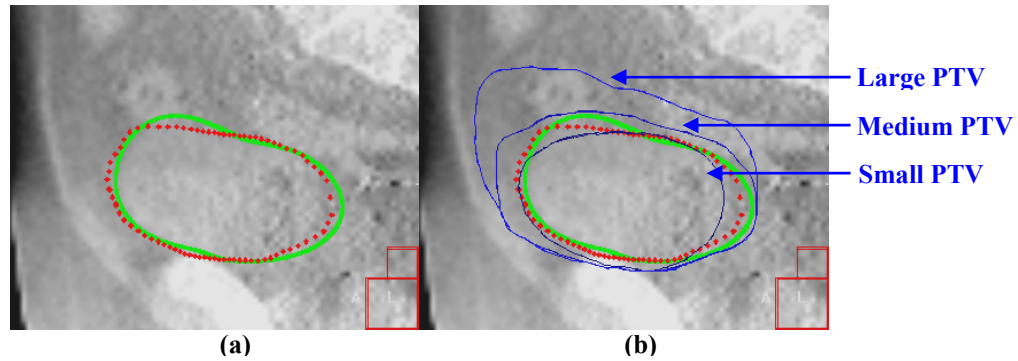


Figure 6.6: (a): The automatically segmented bladder contour (green thick solid curve) and manually delineated bladder contour (red thick dashed curve) were overlaid on a sagittal section of a localization CBCT image. (b): Small, medium and large PTVs (blue thin curves) from the library of plan were overlaid on top on (a). In this example, the medium PTV was the smallest PTV safely covering the entire bladder volume, hence, the medium PTV was selected as the plan of the day.

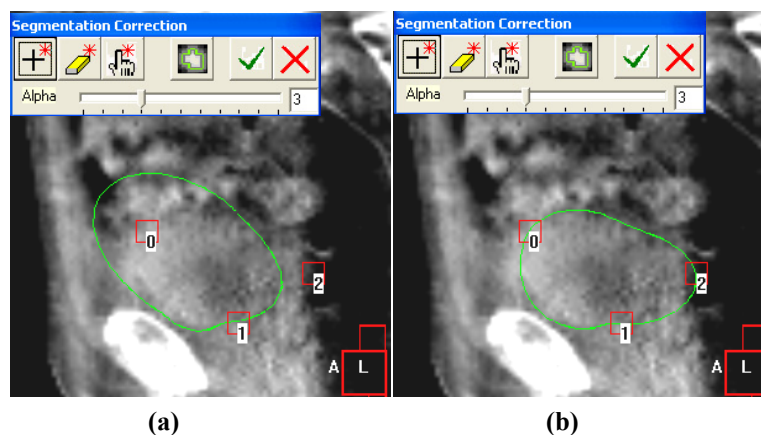


Figure 6.7: (a): Three markers were manually added on the border of bladder to correct the incorrectly segmented bladder. (b): After including these markers into the cost function, the segmentation result was correct.

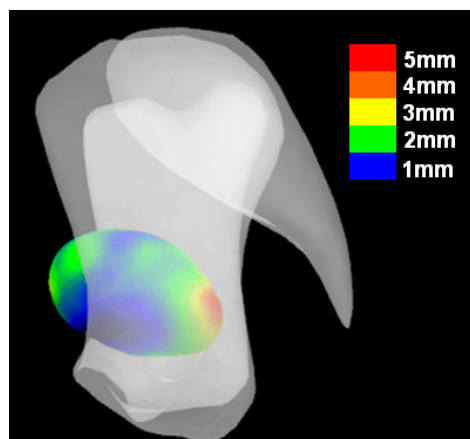


Figure 6.8: Visualization of the global average residual error distribution over all 233 bladder segmentations.

The median, 10th percentile and 90th percentile of CI overlap indices, and SD of signed residual errors for each patient of both automatic and semiautomatic segmentation methods were plotted in figure 6.9 and figure 6.10. It is observed that the semiautomatic segmentation method, if used, always yielded a higher overlap and lower residual error than the automatic segmentation method. In general, for the automatic segmentation method, the mean CI overlap index and SD residual error over all 233 segmentations are 70.5%, and 0.41 cm, respectively. After the correction step, CI overlap indexes increased to 77.7%, while the mean residual error reduced to 0.30 cm (table 6.1).

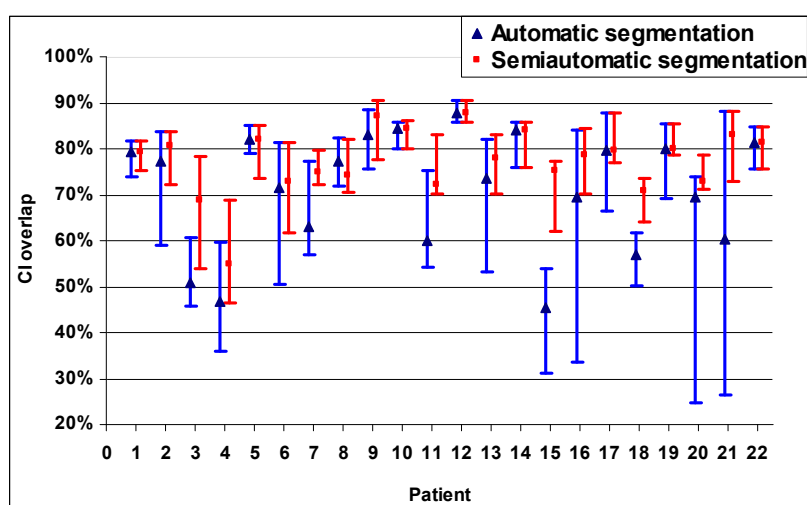


Figure 6.9: The median (triangle), 10th percentile (minus error bar) and 90th percentile (plus error bar) of CI overlap indexes between automatically segmented bladder and manually delineated bladder, and the median (square), 10th percentile (minus error bar) and 90th percentile (plus error bar) of CI overlap indexes between semi-automatically segmented bladder and manually delineated bladder for all 22 patients.

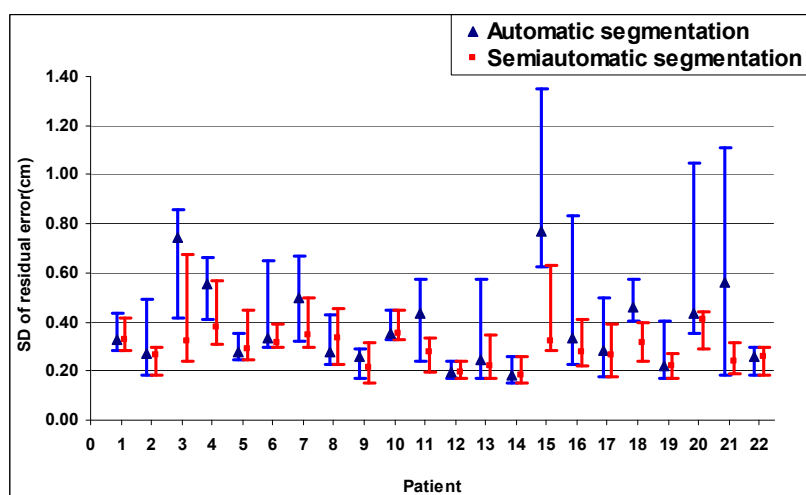


Figure 6.10: The median (triangle), 10th percentile (minus error bar) and 90th percentile (plus error bar) of the SD of signed local residual error for automatic bladder segmentation method and the median (square), 10th percentile (minus error bar) and 90th percentile (plus error bar) of the SD of signed local residual error for semiautomatic bladder segmentation method for all 22 patients.

Table 6.1: Mean CI overlap and mean residual error (SD of signed distance) of the automatic and semiautomatic bladder segmentation methods.

	Mean CI Overlap	Mean residual error (cm)
Automatic segmentation	70.5%	0.41
Semiautomatic segmentation	77.7%	0.30

The mean and SD of the volume difference of automatic and manual bladder segmentations are 7.3 ml and 73.3 ml. The mean and SD of the volume difference of semiautomatic and manual bladder segmentation are -1.8 ml and 25.5 ml. Since the mean volume difference is very small, the mean signed residual errors over all 22 patients for both are almost zero (<0.03 cm).

The mean bladder volume in the training data set is 221 ± 115 ml (1SD). For the validation data set, the mean bladder volume of 14 patients with the full bladder protocol was 256 ± 220 ml (1SD), while the mean volume of the 8 patients with the empty bladder protocol was 121 ± 34 ml (1SD). We did not find a difference in the segmentation accuracy between full and empty bladders: mean residual errors for full and empty bladders were 0.28 cm and 0.31 cm, respectively ($p=0.10$, paired t-test). However, since the overlap indices are very sensitive to volume, the CI overlap for full bladder is significantly higher than that for empty bladder ($p<0.01$, paired t-test). The mean CI overlap indices for full and empty bladder are 78.9% and 75.4%, respectively.

The agreement between the selections made by manual and fully automatic bladder segmentations was 56.7% (figure 6.11). In 31.8%, 8.2% and 3.4% of the cases, the plan selected by automatic segmentation was respectively one size, two sizes and three sizes different from the plan selected by manual delineation. With after manual correction, the plan selection agreement improves to 80.7%. The plans selection disagreement between semiautomatic segmentation and manual delineation was 17.6% for one size difference, 1.7% for two sizes difference and 0% for three sizes difference.

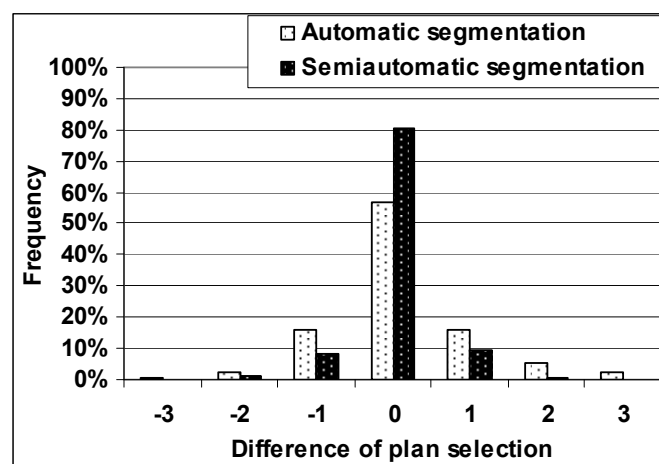


Figure 6.11: Histogram of the difference between the plans selected by the two segmentation methods and plans selected using the manually delineated bladder. Zero on the x axis means that same plan was selected. The other non-zero numbers in x axis indicate difference of PTV size of the plans selected by manual delineation and two segmentations methods., e.g. when a plan for large PTV was selected by manual delineation, while a plan for medium PTV was selected by automatic segmentation, the difference of plan selection was -1.

6.5 Discussion

We presented a novel method for semiautomatic bladder segmentation on CBCT. Using a population data as prior knowledge, this method avoids unrealistic bladder segmentation shapes and produces an automatic bladder segmentation in a short time with moderate accuracy (70.5% mean CI overlap). After the automatic segmentation, a quick manual correction can be performed to correct the poorly segmented bladders. This manual correction improves the mean CI overlap of bladder segmentation to 77.7%, which is similar to the inter-observer variability of bladder delineation on CBCT reported in literatures, that are 75.0% CI overlap from Foroudi et al. [126] and 82% CI overlap from Lutgendorf-Caucig et al. [127].

We first modeled the bladder shape using spherical harmonic expansion. The advantage of this step is that it suppresses high spatial frequencies that are not expected in the bladder. If we would directly perform principal component analysis on the Cartesian space of all the training bladder contours, delineation error and re-sampling error would introduce unrealistic high spatial frequencies in the dominating PCA modes. One study used spherical harmonics with 10-20 degrees to model the bladder [135]. Although higher degrees can lead to more accurate modeling, in our data the average residual fitting error with 5 degrees is already smaller than the voxel size, so we favor less degrees for the sake of computation speed.

The automatic segmentation method uses a population based model as prior knowledge, in combination with the bladder contour and image gradients of the planning CT. These data are always available for radiotherapy patients, as they are standard input for the IGRT process. In general segmentation applications, such data is not available. The combination of population based prior information from a large training data set with patient-specific prior information from the planning CT is a powerful method to segment the bladder on CBCT.

One assumption of the automatic segmentation is that the image gradients around the bladder in the planning CT are highly correlated with the gradient value on the corresponding location in the localization CBCT. However, because this correspondence is currently defined along the radial direction large deformation or shifts invalidate this assumption. In addition, resolution differences as well as noise and artifacts lead to inconsistencies. We defined the cross correlation between the sampled gradient fields of CT and CBCT images as cost function. Although the optimal value of the cost function is far from zero, it still captures the image contrast.

In 72 out of 233 localization CBCT images, the automatic segmentation had a very low similarity with the manual delineation (CI overlap <0.65). This typically occurs because a local minimum is found by the simplex optimizer. To deal with this problem, we have a limited manual intervention. For online bladder segmentation just before treatment, a visual assessment by the radiographer is always necessary to ensure high quality segmentation for the plan selection in the next step. After automatic segmentation, the user usually roams through the sagittal plans of the localization CBCT and visually checks whether the bladder contour fits the edge of bladder. Where the user observes contour mismatches, a few markers are placed. In practice, we suggest the users to place a pair of markers each time instead of a single marker, i.e. one marker locates on the mismatched edge of the bladder and the other is

on the opposite side of the edge of the bladder. Such marker pairs avoid over-correction problems in practice.

The agreement between the selections made by manually delineated and automatically segmented bladders is 56.7%, while manual correction improves the agreement to 80.7%, which is higher than the reported agreement between different observers (range from 70% to 77% [23;55;116]). The mean segmentation and plan selection time including manual correction is about half a minute, which is shorter than the average 1.5 minutes plan selection time reported by Lalondrelle et al. [23]. So the semiautomatic segmentation provides a faster plan selection tool with the same accuracy as manual selection, and therefore can facilitate clinical implementation of multiple plan ART of bladder cancer.

In a previous study, we built a patient-specific bladder model based on the first six images of each patient to guide the segmentation. That method is more robust to the image artifacts. However, when the bladder in the localization CBCT has a different deformation pattern as the bladders in the first six images, the patient-specific model cannot fit to the right bladder shape. In the current study, the population based bladder model gives a general description of inter- and intra- patient bladder deformation, hence it can very well fit the bladder shapes on which the previous method failed. The drawback of the current segmentation method is that the reference planning CT has different gradient values on the bladder edge from the localization CBCT. Moreover, using only one planning CT as the reference image and a simplex optimizer can yield a non-global optimization. To deal with these problems, we manually defined markers to correct the non-global optimization.

From 2007, most patients in our department received a lipiodol (liquid marker) injection on bladder wall via cystoscopy before planning, which was used for both tumor demarcation and image guidance [33;81;129]. However, these patients were excluded from our study. That is because the part of the bladder wall with markers has much higher gradient values than other parts, hence it dominates the cost function. When the markers do not move along the radial direction, the segmentation is incorrect. In other words, the image data with lipiodol on bladder wall is not compatible with the automatic segmentation algorithm. A simple way to deal with the images with lipiodol is to set α to a very large value such that it only uses the markers without image information to determine the cost function. We have found that about 30 markers are needed to produce a good bladder segmentation without using imaging information. This is very similar to the segmentation approach proposed by Price et al. [135].

The training data for building bladder model is 95 bladder contours from 8 patients with full bladder drinking protocol, while the segmentation method was validated on the data of 22 patients with both full and empty bladder drinking protocols from a different institute. This finding suggests that our segmentation method is not very dependent on drinking protocols or CBCT image acquisition protocols.

One limitation of current bladder segmentation method is that it has only been trained on, and therefore works on, male patients. Since about 70% of muscle invasive bladder cancer patients in our hospital are male patients, we have first built a generic

male bladder model. A female bladder model will be built for bladder segmentation on female patients in the future.

6.6 Conclusion

PCA on spherical harmonics space is an efficient method to describe bladder deformation. The statistical shape based segmentation approach is robust to the relatively poor CBCT image quality and allows automatic segmentation of bladder on CBCT with moderate accuracy. A limited user intervention quickly and reliably corrects failed segmentations. This segmentation method is suitable to select the appropriate plan for a multiple plan ART of bladder cancer.